PAPER • OPEN ACCESS

Hydrogenated ultra-thin tin films predicted as two-dimensional topological insulators

New Journal of Physics
The open access journal at the forefront of physics
Deutsche Physikalische Gesellschaft DPG | IOP Institute of Physics

Hydrogenated ultra-thin tin films predicted as two-dimensional topological insulators

Bo-Hung Chou[1], Zhi-Quan Huang[1], Chia-Hsiu Hsu[1], Feng-Chuan Chuang[1], Yu-Tzu Liu[2], Hsin Lin[2] and Arun Bansil[3]

[1] Department of Physics, National Sun Yat-Sen University, Kaohsiung 804, Taiwan
[2] Graphene Research Centre and Department of Physics, National University of Singapore, 117542, Singapore
[3] Department of Physics, Northeastern University, Boston, Massachusetts 02115, USA
E-mail: fchuang@mail.nsysu.edu.tw and nilnish@gmail.com

Received 22 May 2014, revised 16 September 2014
Accepted for publication 24 September 2014
Published 7 November 2014

New Journal of Physics **16** (2014) 115008

doi:10.1088/1367-2630/16/11/115008

Abstract

Using thickness-dependent first-principles electronic structure calculations, we predict that hydrogenated ultra-thin films of tin harbor a new class of two-dimensional (2D) topological insulators (TIs). A single bilayer (BL) tin film assumes a 2D-TI phase, but it transforms into a trivial insulator after hydrogenation. In contrast, tin films with 2 and 3 BLs are found to be trivial insulators, but hydrogenation of 2 to 4 BL films results in a non-trivial TI phase. For 1 to 3 BLs, H-passivation converts the films from being metallic to insulating. Moreover, we examined iodine-terminated tin films up to 3 BLs, and found these to be non-trivial, with the films becoming semi-metallic beyond 1 BL. In particular, the large band gap of 340 meV in an iodine-terminated tin BL is not sustained in the iodine-terminated 2 BL and 3 BL tin films.

Keywords: 2D topological insulators, topological phase transition, quantum spin hall effect, tin thin films, electronic structures, first-principles calculations

Introduction

Two-dimensional (2D) topological insulators (TIs) or quantum spin hall (QSH) insulators are characterized by the presence of gapless edge states protected by the constraints of time-reversal symmetry in an otherwise insulating bulk material [1–3]. The spin polarized conducting channels at the edges of a 2D-TI are free from backscattering, promising low power consuming applications. The materials realization of QSH insulators is, however, limited currently to HgTe/CdTe [4–6] and InAs/GaSb/AlSb [7, 8] quantum well systems with small band gaps of 4 $\sim$ 10 meV. The need for finding new 2D TI materials with larger band gaps, which could support room-temperature applications, is thus clear.

Recent progress in search of new QSH insulators has been made by considering counterparts of graphene [9] in group IVA (IV) and group VA (V) elements of the periodic table. First-principles calculations predict that freestanding, single layer thick films of Si (silicene) [10, 11], Ge (germanene) [10, 11], Sn (stanene) [12], and Bi [13–15] in the buckled honeycomb structure are 2D QSH insulators, while an Sb [16, 17] bilayer becomes topologically non-trivial under tensile strain. Furthermore, III–V compounds are a natural extension of Si, and GaBi, InBi, and TlBi thin films are predicted to be 2D TIs [18]. In addition to single bilayers, multi-layer Bi (111) films are predicted to be topologically nontrivial for a wide range of film thicknesses [15], suggesting that non-trivial phases could also emerge as a function of film thickness. Although Pb possesses the largest spin–orbit coupling (SOC) strength among the group IV elements, its freestanding one BL thick film turns out to be topologically trivial [11]. Turning to Sn, which is the group IV element with the second largest SOC strength, freestanding Sn exhibits a larger nontrivial band gap than Si or Ge, and has been the subject of a number of previous studies [19]. Tin compounds SnX (X = H, I, Br, Cl, F or OH) in one BL thick layers are predicted to be QSH insulators, with the hydrogenated version called stanane [19]. Hybridization with X atoms removes p_z orbitals from the Fermi energy, so that low-energy states are dominated by other p- and s-orbitals, and the band topology is controlled by a band inversion at Γ as in three dimensional (3D) gray Sn. An insulating gap as large as 300 meV is predicted in SnI. To our knowledge, the thickness dependence of topological properties of Sn thin films has, however, not been addressed in the literature.

In this article we discuss how the crystal and electronic structures of Sn films evolve with film thicknesses up to 10 BLs, including effects of H-passivation and iodine-termination. Our focus is on identifying topological characteristics of the electronic structures of the films. In particular, we predict the existence of non-trivial 2D TI phases in 2 BL and 3 BL stanane films. These two new 2D TIs identified here possess band gaps that exceed thermal energy at room-temperature, making them suitable for room-temperature spintronics applications.

Methods

Calculations were carried out within the generalized gradient approximation (GGA) to the density-functional theory [21, 22] using the projector-augmented-wave method [23] as implemented in the vienna ab-initio simulation package [24]. The kinetic energy cutoff was set at 400 eV and atomic positions were relaxed until the residual forces were less than 10^{-2} eV Å^{-1}. The criteria for achieving self-consistency in electronic structure calculations was set at 10^{-6} eV. In order to model the single bilayer, a vacuum of at least 20 Å was included along the z

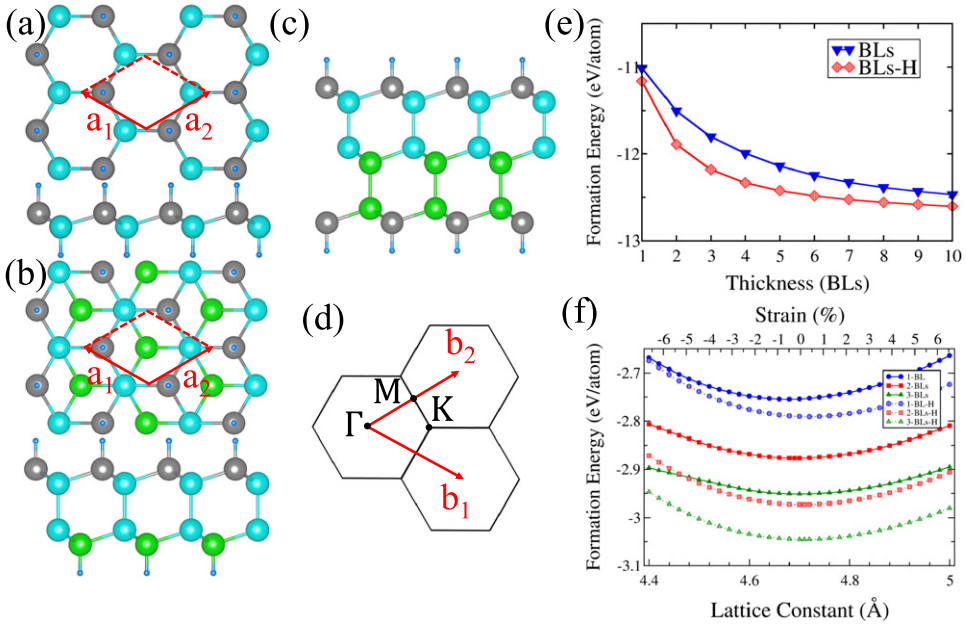

Figure 1. Top and side views of the hydrogenated 1 BL (a) and 2 BL (b) films. (c) Side view of the hydrogenated 3 BL film; top view is similar to that of a 2 BL film in (b). (d) 2D BZs with specific symmetry points labeled. (e) Formation energy as a function of film thickness for pure and H-passivated films. (f) Formation energy as a function of lattice constant for various films; associated strains (with respect to the bulk lattice constant) are shown on the top horizontal scale.

direction. A Γ-centered 12 × 12 × 1 Monkhorst–Pack grid [25] was used to sample the 2D Brillouin zone (BZ).

All crystals investigated in this study are inversion symmetric, which allowed us to assess topological characteristics of their band structures by analyzing parities of energy levels at time-reversal invariant symmetry points in the BZ [3]. The Z_2 invariant, ν, can then be computed from products $\delta(K_i)$ of parities of valence states at the four time-reversal invariant k-points (K_i) via the equations

$$\delta(K_i) = \prod_{m=1}^{N} \xi_{2\,m}^{i} \quad ; \quad (-1)^{\nu} = \prod_{i=1}^{4} \delta(K_i), \tag{1}$$

where $\xi = \pm$ are the parity eigenvalues of Kramer's doublets and $2N$ is the number of valence bands.

Results and discussion

3D bulk α-Sn is a semimetal with a diamond structure. The Sn films we investigated are obtained from the bulk α-Sn lattice by taking a 2D slice perpendicular to a (111) direction. One BL consists of two Sn atoms in one unit cell of the buckled honeycomb structure. Unit cells of hydrogenated Sn (111) ultra-thin films and the associated 2D BZs are shown in figures 1(a)–(d). After constructing pure (un-hydrogenated) as well as hydrogenated Sn (111) thin films, we optimized all atomic positions using a symmetric constraint in all cases.

In order to compare relative stabilities of films of various thicknesses, we define the formation energy, E^f, as

$$E^f = \left(E_{\text{tot}} - N_{\text{Sn}} \times \mu_{\text{Sn}} - N_{\text{H}} \times \mu_{\text{H}}\right) / N_{\text{Sn}}\,, \tag{2}$$

where E_{tot} is the total energy of the film. μ_{Sn} and μ_{H} are chemical potentials of Sn and H, respectively. N_{Sn} and N_{H} denote numbers of Sn and H atoms. We take μ_{H} to be half of the total energy, E_{H_2}, of a single hydrogen molecule, and μ_{Sn} to be the calculated total energy of an isolated Sn atom. Note, however, that values of μ_{Sn} and μ_{H} could be taken from isolated atoms, molecules or solids as long as a single element is involved. The different choices only introduce a constant shift in the total energy, but the relative energy differences between films with different numbers of layers, with or without decorations, which are our focus in this study, remain unchanged.

The formation energy as a function of lattice constant, a, is plotted in figure 1(f) for various Sn (111) films with and without H-passivation. Equilibrium lattice constants of pure films are found to be 4.68, 4.69, and 4.70 Å for 1, 2, and 3 BLs, respectively, while the corresponding values for the hydrogenated films are 4.72, 4.71 and 4.71 Å. The hydrogenated films are seen to be energetically more stable compared to the corresponding unhydrogenated films. The equilibrium lattice constant of the 3 BL film is quite close to the bulk value of 4.716 Å. For this reason, for films greater than 3 BL thickness, we fixed the lattice constant to the bulk value, and only allowed the atomic positions to relax. The formation energy as a function of the number of BLs is shown in figure 1(e). We see that as the thickness increases, the formation energy monotonically decreases to a limiting value.

Note that the Z_2 topological invariant is well defined only for insulating or semi-metallic band structures where conduction and valence bands are separated at all k-points. The band topology is ill-defined in metallic systems with mixed conduction and valence bands. In fact, our band structures for Sn films with four or more BLs, and for stanane films with five or more BLs present such mixed band structures. For this reason, we examined the topologies of Sn films only up to 3 BLs, and of stanane films up to 4 BLs. With reference to equation 1, results of parity analysis at the four time-reversal invariant symmetry points in these films and the resulting Z_2 invariants are summarized in table 1. For pure films, 1 BL film is non-trivial, but 2 BL film is trivial. Our analysis shows that the 3 BL film is trivial at zero strain, but becomes non-trivial under a compressive strain at $a = 4.63$ Å. On the other hand, for hydrogenated films, 1 BL film is trivial, but 2 BL film is non-trivial and undergoes a topological phase transition to a trivial phase at $a = 4.687$ Å. Furthermore, the hydrogenated 3 BL film is non-trivial over the entire range of strains we considered ($a = 4.62$ Å to $a = 4.88$ Å). Hydrogenated 4 BL film is a non-trivial semimetal. Thus, the insulating phase in hydrogenated films is limited to at most 3 BLs.

In order to gain insight into the nature of band inversion in the films, we investigated band structures with and without the SOC in a number of cases. We also considered the evolution of band structures as a function of strength of the SOC by adding a weighting factor WSOC to scale the SOC contribution in the computations. Figure 2 presents illustrative results for H-passivated 2 and 3 BL films, which as we have already discussed, are non-trivial for at optimized structures. In the 2 BL stanane film (top row of figure 2), the band gap is seen to close and then reopen at the Γ point with increasing SOC strength, resulting in a band inversion. Note that the sizes of red circles in figure 2 are proportional to the contribution of the s-orbital to the wave function. A band inversion can be monitored by observing that the red circle at the bottom

Table 1. Parity δ (see equation (1)) at the Γ and three-fold M points and the Z_2 invariant of pure (stanene) of H-passivated (stanane) films of various thicknesses at optimized structures. I denotes an insulator and M a metallic state.

	Stanene		
No. of BLs	1	2	3
$\delta(\Gamma)$	+	+	−
$3\,\delta(M)$	−	+	−
ν	1	0	0
Insulator/metal	I	M	M

	Stanane			
No. of BLs	1	2	3	4
$\delta(\Gamma)$	+	−	−	−
$3\,\delta(M)$	+	+	+	+
ν	0	1	1	1
Insulator/metal	I	I	I	M

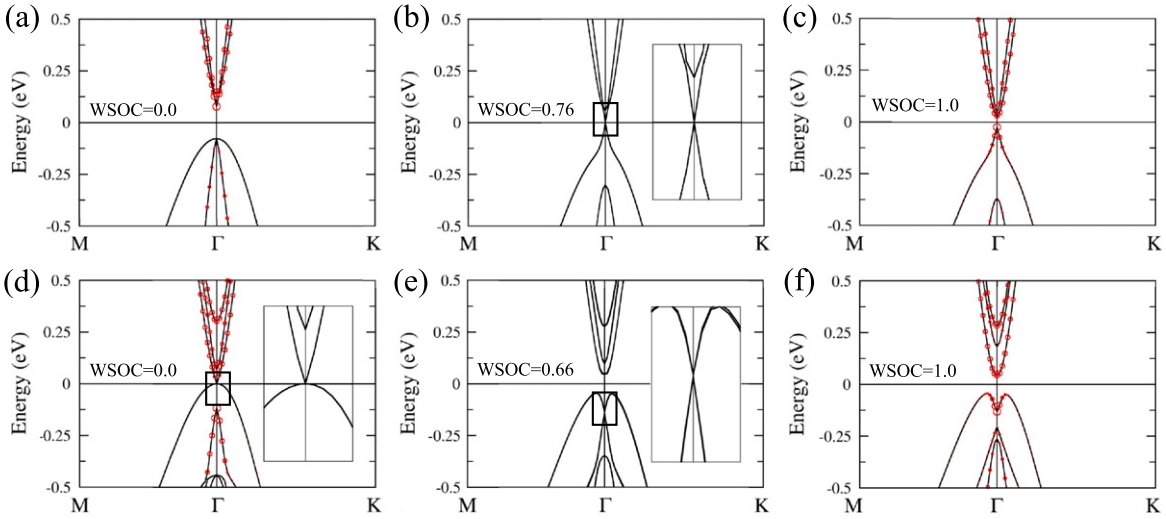

Figure 2. Band structures of 2 BL (top row) and 3 BL (bottom row) stanane films for various strengths of the SOC, obtained by weighting the strength of the SOC in computations via the scaling parameter WSOC. Values of WSOC are indicated in various panels. The sizes of red circles are proportional to the contributions of s-orbital to the wave functions.

of the conduction band at WSOC = 0 moves to the top of the valence band at WSOC = 1. The system thus undergoes an SOC driven topological phase transition with the critical point at WSOC = 0.76 when the conduction and valence bands meet at Γ. This critical phase could perhaps be realized via alloying effects on the electronic structure [26, 27] using an element such as Ge with a smaller SOC strength than Sn.

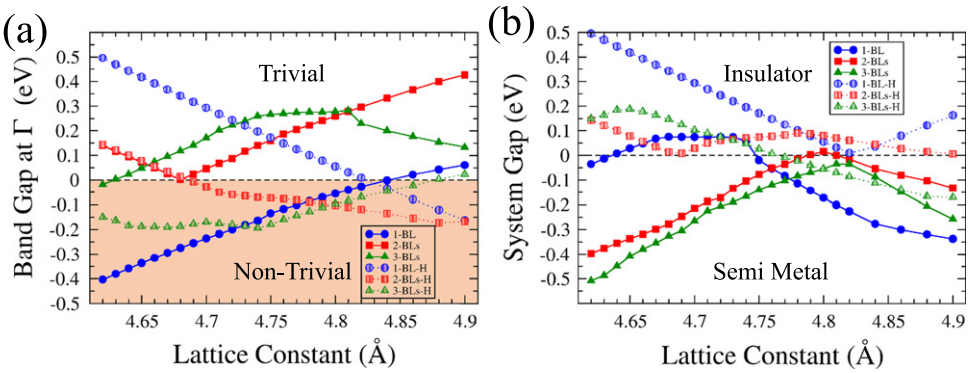

Figure 3. (a) Band gaps at Γ in passivated and unpassivated Sn films as a function of the lattice constant. Films with positive gap values are in the trivial phase, while those with negative values (shaded) are non-trivial. (b) Same as (a), except that the system gap is shown, which is defined as the difference in the energy of the lowest level in the conduction band and the highest level in the valence band. Positive gap values indicate an insulating band structure, and negative values a semimetal phase.

Turning to the 3 BL H-passivated Sn film (bottom row of figure 2), we see that it is a semimetal in which the conduction and valence bands are inverted and meet at Γ for WSOC = 0, figure 2(d). When SOC is turned on, no matter how small, a gap opens up at Γ and a QSH insulating phase emerges as seen in figure 2(e) for WSOC = 0.66. Note that there is no change in the band topology of the 3 BL stanane film with increasing strength of the SOC, and unlike the 2 BL case, the 3 BL film does not undergo a topological phase transition. The behavior of 2 BL and 3 BL stanane films is thus quite different in that the SOC is responsible for inducing band inversion in the 2 BL film, but it opens the band gap in the 3 BL film. Nevertheless, in both films, the non-trivial phase is driven by a band inversion at the Γ point.

In this connection, note that in figures 2(a) and 2(d) where the SOC is set to zero (WSOC = 0), the s-orbital contribution to the highest valence level at the Γ point vanishes. When the full SOC is turned on (WSOC = 1) the corresponding figures 2(c) and (f) show that a substantial s-weight now moves below the Fermi level. A similar analysis of the p-spectral weight shows an opposite trend when the SOC is turned on (not shown in the interest of brevity). Finally, we examined the d-spectral weight, and found it to be essentially zero around the Fermi energy with or without the SOC. In this way, we adduce that the inversion involved in the present case is between the s and p orbitals.

Bearing the preceding discussion of band structure in mind, the band topology of stanane films can be monitored via the direct band gap, E_g^Γ, at the Γ point. E_g^Γ is defined to be negative when the band gap is inverted. Films with negative values of E_g^Γ are thus non-trivial, while those with positive values are trivial insulators. At zero strain, E_g^Γ is negative for 1 BL stanene as well as for 2 and 3 BL Sn films. As demonstrated previously for Sb and Bi bilayers [14, 17], it is possible to change band topology via strain. Along this line, values of E_g^Γ as a function of strain are shown in figure 3(a) for various Sn and stanane films, highlighting how strain can drive topological phase transitions in these films. Pure 2 BL and 3 BL films as well as 1 BL stanane are seen to be in the trivial phase. Hydrogenated 2 BL film is non-trivial at its optimal structure, but transforms into a trivial phase at a = 4.687 Å. Unhydrogenated 1 BL and

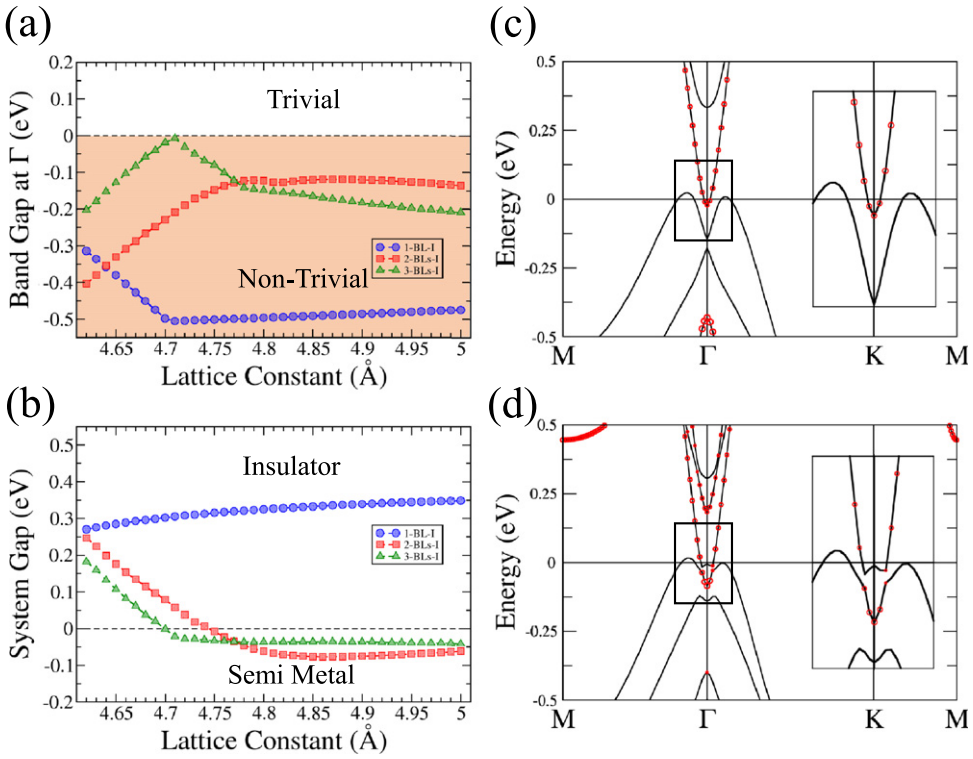

Figure 4. (a) Band gaps at Γ and (b) the system gaps of iodine-terminated Sn films as a function of the lattice constant. (c) and (d) are band structures of iodine-terminated 2 and 3 BL films, respectively.

hydrogenated 3 BL films remain in non-trivial phase over a wider range of strains, transforming into trivial insulators under tensile strain at $a = 4.84$ Å and $a = 4.88$ Å.

It is interesting to consider what may be called a system band gap, defined as the energy difference between the lowest energy level of the conduction bands and the highest level of the valence bands, see figure 3(b). Positive values of such a system gap imply an insulator, while negative values indicate a semimetal state. The system gap is more relevant for transport applications than the band gap at Γ considered in figure 3(a). For example, even though the inverted gaps at Γ in figure 3(a) in 1 BL Sn films are as large as 244 meV, the corresponding system gaps in figure 3(b) are only about 60 meV.

Finally, we discuss effects of iodine decoration on Sn films. A 1 BL thick SnI film possesses a band gap as large as 0.34 eV [19]. Here we consider iodine adsorbed on surfaces of 1–3 BL Sn films. The optimized lattice constants are found to be 4.91, 4.78, and 4.75 Å for the 1, 2, and 3 BL iodine terminated films, respectively. Our parity analysis indicates that iodine-terminated 1–3 BL films are all non-trivial with an inverted band gap at Γ, see figure 4(a). Notably, even though the band gap closes at about 4.71 Å in the iodine-terminated 3 BL Sn film, there is no topological phase transition over the entire range of strain considered, since parities of all the states at the Γ point around the Fermi energy are the same (i.e. odd). Unfortunately, however, iodine-terminated 2 and 3 BL films are semimetals with a negative system gap. In contrast, the system gap in a 1 BL film is 0.34 eV, see figure 4(b). In other words, iodine is a useful decoration only in the 1 BL Sn film. Incidentally, our analysis shows that the band inversion involved in the I-passivated 2 BL and 3 BL films is of s–p type.

We have carried out test computations based on the hybrid functional HSE06 [28] to assess the robustness of our results. For this purpose, we chose two lattice constants as exemplars, one around the equilibrium lattice constant of the LB phase ($a < 4.72$ Å) and the other after the phase transition ($a > 4.9$ Å), and repeated the calculations using the HSE06 functional. These calculations show that our GGA based results correctly capture the evolution of topological phases with strain in H- and I- passivated Sn films, some differences in the exact values of the strain at which phase transitions occur notwithstanding.

Conclusions

To summarize, using first-principles electronic structure calculations, we predict a new class of 2D-TIs among the hydrogenated ultra-thin Sn films (stananes) with band gaps large enough for room temperature applications. A 1 BL pure Sn film is a 2D-TI, but becomes a trivial insulator after hydrogenation. 2 BL and 3 BL pure films, on the other hand, are trivial, but transform into a non-trivial phase upon hydrogenation with band gaps as large as 244 meV without strain. The topological phases in stananes are controlled by band inversion at the Γ-point. In the 2 BL stanane film, SOC drives the band inversion at Γ, while in the 3 BL stanane film, SOC only opens the band gap at Γ, but does not otherwise change the band topology. Our study suggests that it should be possible to realize novel 2D-TI phases by growing ultra-thin Sn films on substrates such as SiC (0001), Si (111) and Ge (111), with the substrate dangling bonds mimicking the role of H-passivation.

Acknowledgements

FCC acknowledges support from the National Center for Theoretical Sciences and the Taiwan National Science Council under Grant Nos. NSC-101-2112-M-110-002-MY3 and NSC-101-2218-E-110-003-MY3. He is also grateful to the National Center for High-performance Computing for computer time and facilities. The work at Northeastern University was supported by the US Department of Energy (DOE), Office of Science, Basic Energy Sciences grant number DE-FG02-07ER46352 (core research), and benefited from Northeastern University's Advanced Scientific Computation Center (ASCC), the NERSC supercomputing center through DOE grant number DE-AC02-05CH11231, and support (applications to 2D materials) from the EFRC: Center for the Computational Design of Functional Layered Materials (CCDM) under DE-SC0012575. H L acknowledge the Singapore National Research Foundation for support under NRF Award No. NRF-NRFF2013-03.

References

[1] Hasan M Z and Kane C L 2010 *Rev. Mod. Phys.* **82** 3045
[2] Qi X-L and Zhang S-C 2011 *Rev. Mod. Phys.* **83** 1057
[3] Fu L and Kane C L 2007 *Phys. Rev.* B **76** 045302
[4] Bernevig B A, Hughes T L and Zhang S C 2006 *Science* **314** 1757
[5] König M, Wiedmann S, Brüne C, Roth A, Buhmann H, Molenkamp L W, Qi X L and Zhang S C 2007 *Science* **318** 766–70
[6] Roth A, Brüne C, Buhmann H, Molenkamp L W, Maciejko J, Qi X L and Zhang S C 2009 *Science* **325** 294

[7] Liu C, Hughes T L, Qi X L, Wang K and Zhang S C 2008 *Phys. Rev. Lett.* **100** 236601
[8] Knez I, Du R R and Sullivan G 2011 *Phys. Rev. Lett.* **107** 136603
[9] Castro Neto A H, Guinea F, Peres N M R, Novoselov K S and Geim A K 2009 *Rev. Mod. Phys.* **81** 109
[10] Liu C C, Feng W X and Yao Y G 2011 *Phys. Rev. Lett.* **107** 076802
[11] Tsai W F, Huang C Y, Chang T R, Lin H, Jeng H T and Bansil A 2013 *Nat. Commun.* **4** 1500
[12] Liu C C, Jiang H and Yao Y G 2011 *Phys. Rev.* B **84** 195430
[13] Wada M, Murakami S, Freimuth F and Bihlmayer G 2011 *Phys. Rev.* B **83** 121310
[14] Huang Z Q, Chuang F C, Hsu C H, Liu Y T, Chang H R, Lin H and Bansil A 2013 *Phys. Rev.* B **88** 165301
[15] Liu Z, Liu C X, Wu Y S, Duan W H, Liu F and Wu J 2011 *Phys. Rev. Lett.* **107** 136805
[16] Zhang P F, Liu Z, Duan W H, Liu F and Wu J 2012 *Phys. Rev.* B **85** 201410
[17] Chuang F C, Hsu C H, Chen C Y, Huang Z Q, Ozolins V, Lin H and Bansil A 2013 *Appl. Phys. Lett.* **102** 022424
[18] Chuang F C, Yao L Z, Huang Z Q, Liu Y T, Hsu C H, Das T and Bansil A 2014 *Nano Lett.* **14** 2505
[19] Xu Y, Yan B, Zhang H J, Wang J, Xu G, Tang P, Duan W H and Zhang S C 2013 *Phys. Rev. Lett.* **111** 136804
[20] Lin H, Das T, Wang Y J, Wray L A, Xu S-Y, Hasan M Z and Bansil A 2013 *Phys. Rev.* B **87** 121202
[21] Hohenberg P and Kohn W 1964 *Phys. Rev.* B **136** 864
Kohn W and Sham L J 1965 *Phys. Rev.* A **140** 1133
[22] Perdew J P, Burke K and Ernzerhof M 1996 *Phys. Rev. Lett.* **77** 3865
[23] Kresse G and Joubert D 1999 *Phys. Rev.* B **59** 1758
[24] Kresse G and Hafner J 1993 *Phys. Rev.* B **47** 558
Kresse G and Furthmüller J 1996 *J. Phys. Rev.* B **54** 11169
[25] Monkhorst H J and Pack J D 1976 *Phys. Rev.* B **13** 5188
[26] Asonen H, Lindroos M, Pessa M, Prasad R, Rao R S and Bansil A 1982 *Phys. Rev.* B **25** 7075
[27] Khanna S N, Ibrahim A K, McKnight S W and Bansil A 1985 *Solid State Commun.* **55** 223
[28] Krukau A V, Vydrov O A, Izmaylov A F and Scuseria G E 2006 *J. Chem. Phys.* **125** 224106